EUROPHYSICS LETTERS 15 April 2006

Europhys. Lett., **74** (2), pp. 306–312 (2006)
DOI: 10.1209/epl/i2005-10523-2

Bouncing transitions on microtextured materials

M. Reyssat[1], A. Pépin[2], F. Marty[3], Y. Chen[2,4] and D. Quéré[1]

[1] *Laboratoire de Physique de la Matière Condensée, FRE 2844 du CNRS Collège de France - 75231 Paris Cedex 05, France*
[2] *Laboratoire de Photonique et Nanostructures (LPN) - Route de Nozay 91460 Marcoussis, France*
[3] *Groupe ESIEE, SMM, Cité Descartes - BP 99, 93162 Noisy le Grand, France*
[4] *Ecole Normale Supérieure - 24 rue Lhomond, 75231 Paris Cedex 05, France*

received 18 November 2005; accepted in final form 14 February 2006
published online 22 March 2006

PACS. 68.08.Bc – Wetting.
PACS. 68.03.-g – Gas-liquid and vacuum-liquid interfaces.
PACS. 68.08.-p – Liquid-solid interfaces.

Abstract. – A drop of water thrown on a super-hydrophobic solid will often bounce off. Here we discuss the conditions to be fulfilled on the surface design (which provides super-hydrophobicity) to observe such a behavior. This allows us to precise how a material can be made water-repellent. We show in particular how the reduction of the scale of the microstructure provides a robust water repellency, and describe some peculiarities of violent shocks on such surfaces.

Super-hydrophobic surfaces are obtained by mixing chemistry (these surfaces are hydrophobic) and physics (they are rough): the presence of a microtexture may enhance dramatically the natural hydrophobicity of the material, yielding contact angles larger than 160° [1]. On such solids, the contact angle hysteresis may be very small (less than 5°), indicating that the liquid (water, here) hardly interacts with its substrate: the drops stand at the top of the microtextures so that there is mainly air below, which explains both large angles and small hysteresis [2]. A convenient way to check these ideas, and to tune finely the wetting behavior of such substrates, consists of decorating a flat solid with micrometric posts, and treating the whole to be hydrophobic. Then, drops are indeed observed to float on the posts [2–4], whose size, distance and height can be varied using photolithography and deep reactive ion etching techniques.

On such substrates, the more dilute the pillars, the larger the proportion of air below the drop, and the higher the contact angle. However, if the pillars are too dilute, they cannot sustain anymore the drop, which falls on the bottom surface. Because the surface roughness is moderate in this limit, the contact angle decreases and becomes close to 90° (its value on a flat hydrophobic surface); on the other hand, the contact angle hysteresis is dramatically increased (owing to the pinning of the liquid inside the cavities), reaching values as high as 100° [5,6]. The water-repellent state is of course the floating one, and it is useful, on a given substrate, to quantify the robustness of this state. This can be done by pressing on the drop

until it sinks in the texture, which provides the critical pressure above which the sticky state is induced [5]. (This transition is always observed to be irreversible, and other control parameters such as light, temperature or electric field were proposed to induce it [7–9].) Similarly, it was shown that depositing small drops and large ones may lead to different states [5]: while a large drop floats, a small one, of high curvature, will tend to sink; once it reaches the bottom, it becomes sticky.

Here we explore what happens when throwing a water drop onto a surface decorated with micropillars: then, a drop can simply bounce back, making these materials literally water-repellent [10]. However, we expect from compression experiments that pinning should happen provided the impact velocity is large enough. Conversely, it must be emphasized that rebounds are only possible if the impact speed V is high enough: because of a small residual hysteresis on these surfaces, energy can be stored while the drop expands and retracts; for a drop of size R and hysteresis $\Delta\cos\theta$ (where θ is a mean contact angle), and denoting γ as the surface tension, the stored surface energy will scale as $\gamma R^2\Delta\cos\theta$, of the order of γR^2. The drop will bounce if its kinetic energy (which scales as ρR^3V^2, with ρ the liquid density) is larger than this surface energy, which means that the velocity must exceed a value of the order of $(\gamma/\rho R)^{1/2}$. This minimum velocity is typically a few tenths of cm/s, corresponding to release heights of a few millimeters: in most usual cases, the drop will fall from much larger heights. If the impact velocity is fixed, these considerations also imply that only "large enough" drops will bounce: for $V = 1\,\mathrm{m/s}$, we find that the critical radius of sticking is of the order of $100\,\mu\mathrm{m}$. This is indeed the case: on such surfaces, millimetric water drops will elastically rebound while drops coming from a spray will not. This sharply contrasts with what can be observed with drops hitting very hot plates. Then, the presence of a vapor film below the drop leads to the ultimate state of non-wetting ($\theta = 180^\circ$ and $\Delta\theta = 0^\circ$). In this so-called Leidenfrost situation, there is no minimum velocity required for having a rebound and it is even found that small impact velocities provide a quasi-elastic bouncing, yielding to sequences of several hundreds successive rebounds [11].

We show in fig. 1 what happens for a water drop of radius $R = 1.2\,\mathrm{mm}$ hitting such a super-hydrophobic solid at a speed of $1\,\mathrm{m/s}$. The surface is made of silicon, and decorated with silicon micropillars of height $h = 10\,\mu\mathrm{m}$, diameter $d = 2.5\,\mu\mathrm{m}$ and inter-pillar distance $\ell = 7.5\,\mu\mathrm{m}$. The whole material is treated with a fluoropolymer, which makes it super-hydrophobic ($\theta = 150^\circ$ and $\Delta\theta = 20^\circ$). The impact is shot with a high-speed camera (the interval between two successive pictures is 5 ms), using backlighting for improving the contrast.

The drop first spreads before retracting. Because the kinetic energy of the impinging drop

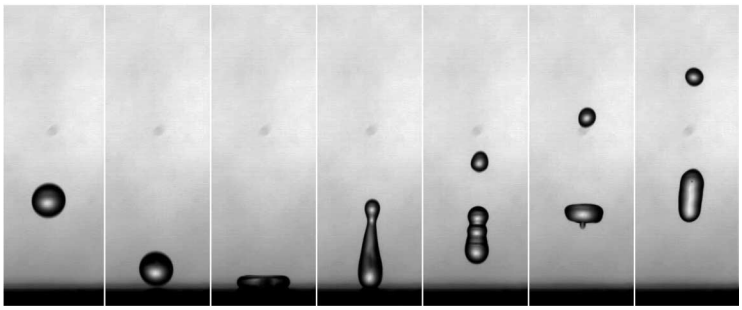

Fig. 1 – Rebound of a millimetric water drop hitting a solid decorated with micrometric hydrophobic posts at a velocity of about 1 m/s. The full drop bounces back, which defines water repellency. The interval between pictures is 5 ms.

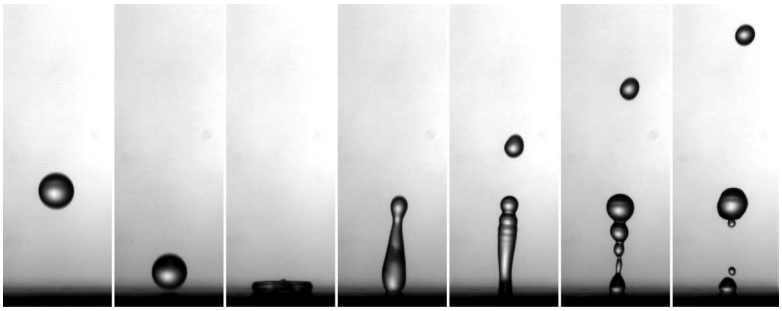

Fig. 2 – Drop hitting a super-hydrophobic substrate (same system as in fig. 1), just above the pinning velocity V^*: part of the drop remains trapped inside the texture, which leads to a partial bouncing. The interval between two pictures is 5 ms.

is here much larger than its surface energy (the ratio between both quantities, referred to as the Weber number $\rho V^2 R/\gamma$, is 15 in this example), the drop considerably deforms as it hits the solid, and as it takes off. This has several consequences: 1) the drop pinches at its top, and ejects a satellite droplet; 2) because the drop is deformed at take-off, part of the kinetic energy is transferred in surface energy, which eventually leads to significant energy losses during the shock (this is quite visible, the drop leaving the solid at a velocity smaller than the impacting velocity). However, the main (practical) result is a dry solid after the shock: the material nicely played its water-repellent role.

Figure 2 shows what happens upon slightly increasing the impact velocity (1.2 m/s, instead of 1 m/s in the previous figure), for a similar drop hitting the same material.

While the four first pictures are comparable to the previous sequence, it is then observed that the bottom of the elongated drop irreversibly pins on (or in) the solid, which modifies the shape of the liquid as it (partially) takes off: a succession of beads is generated, which creates supplementary satellites. We denote as V^* the velocity above which such pinning takes place.

These observations can be completed by top views in the spreading stage. Figure 3 shows such a view, taken 5 ms after a drop of radius $R = 2$ mm impacts at $V = 1.8$ m/s the same surface as used in figs. 1 and 2. The Weber number is 100, so that the drop largely expands, until it reaches a radius of about 7 mm (fig. 3 captures this stage of maximum extension).

The drop, as it expands, forms a transparent sheet bounded by a liquid rim (as observed for a jet impacting a solid target). But the remarkable (and new) point is the occurrence, at

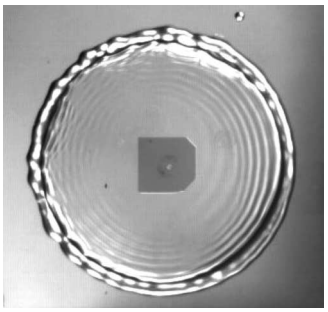

Fig. 3 – Top view of a drop impacting at $V > V^*$ ($V = 1.8$ m/s and $V^* = 1.1$ m/s) a super-hydrophobic substrate decorated with a square lattice of micropillars. A dark square zone (of side 3 mm) at the center of impact reveals that water has there penetrated the texture.

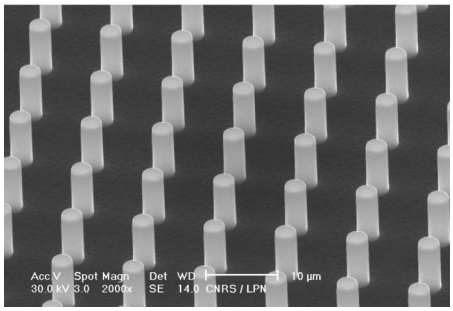

Fig. 4 – Microphotograph (taken with a scanning electron microscope) showing a typical texture made for this study. The posts and bottom substrate are made of silicon, and coated with a fluoropolymer. For this particular texture (on which the experiments displayed in fig. 1, 2 and 3 were made), the pillars diameter, height and distance are 2.5, 10 and 7.5 μm, respectively. The bar indicates 10 μm.

the center of impact, of a (nearly) square dark zone: this proves that at this place, the drop has sunk inside the texture, leading to a darkening of the solid. Taking at the same time a side view of the shock confirms that such a penetration efficiently pins the drop: the bottom of the elongated drop is trapped on a diameter equal to the size of the square. We can finally notice the presence of a tiny white spot at the very center, which betrays the trapping of a small (air) bubble at impact.

The shape of the pinned zone directly reflects the design of the microtextures. We display in fig. 4 a photograph (taken with a scanning electron microscope) of the substrate used in fig. 3: the pillars form a regular array, with a square pattern, so that pinning is favored along the rows of pillars. Note also in fig. 3 the defects on the right side of the square: owing to the large energy stored in corners, oblique frontiers are there more favorable.

The threshold velocity V^* above which pinning occurs was determined for many different samples such as the one displayed in fig. 4. In all the cases, the materials were etched in silicon and coated with the same fluoropolymer, and the pattern chosen to be square arrays of cylindrical pillars. The pillar diameters were roughly constant (around 2 μm), but both the height h and distance between pillars ℓ were varied, from 4 to 35 μm for the first quantity, and between 3 and 26 μm for the second one. For all these substrates, a drop gently deposited is observed to sit at the top of the posts. V^* was in general unambiguously determined (within a typical error less than 5%), and all the results are collected in fig. 5, where the dynamic pressure at the threshold ρV^{*2} is plotted as a function of $\gamma h/\ell^2$, a characteristic Laplace pressure associated with the drop deformation inside the textured material. Note that the values of these parameters for the experiment displayed in fig. 3 are 3 kPa and 11 kPa, respectively, showing in fig. 5 that we are clearly in the pinning region.

In this representation, all the data collapse along a single line, which defines a phase diagram: the drop pins above the line, while the material behaves as water-repellent below it. This might suggest an interpretation for the pinning transition. As it hits the solid, the drop exerts a dynamic pressure which scales as ρV^2. For an inter-pillar distance ℓ, a natural penetration (and thus sticking) pressure might be γ/ℓ. Then, the threshold velocity should be of the order of $(\gamma/\rho\ell)^{1/2}$, independent of h, the pillar height. This is not true: it is observed in fig. 5 that for a series of samples of a given ℓ (corresponding to a given symbol), increasing h makes the threshold velocity increase (logically, long pillars better resist water penetration than small ones). This might be due to the deformation of the liquid/vapor interface below the drop, which implies a Laplace pressure scaling as $\gamma\delta/\ell^2$ (for interface deformations δ smaller

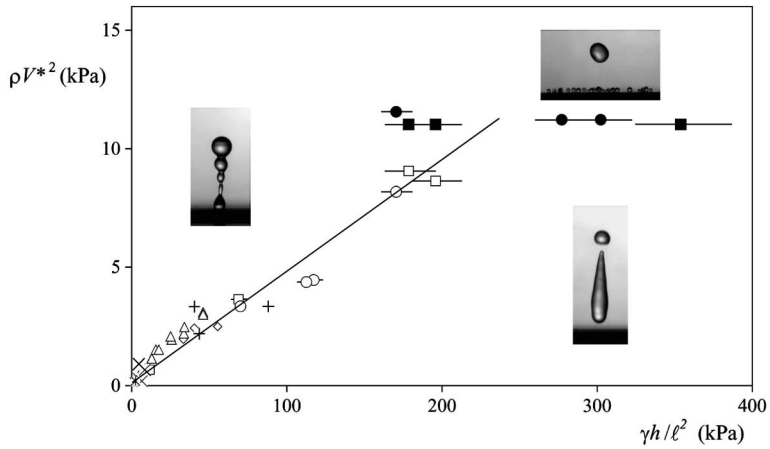

Fig. 5 – Threshold impact velocity V^* of the pinning, as a function of the size of the microtextures (h and ℓ are the height and mutual distance of pillars). Both quantities are expressed as pressures (ρ and γ are the liquid density and surface tension). The symbols correspond to different ℓ: $\square$ $\ell = 3\,\mu$m ($h = 7$, 12, 17, 26 μm); $\circ$ $\ell = 4\,\mu$m ($h = 11$, 21, 29, 33 μm); $\diamond$ $\ell = 5\,\mu$m ($h = 14$, 20 μm); $+$ $\ell = 6\,\mu$m ($h = 20$, 23, 37 μm); $\triangle$ $\ell = 8\,\mu$m ($h = 4$, 6, 10, 14, 19, 26, 35 μm); $\times$ $\ell = 18\,\mu$m ($h = 5$, 11, 18, 24, 36 μm); $*$ $\ell = 26\,\mu$m ($h = 14$, 20 μm). Below the line, the drop bounces back (water repellency), while it is partially pinned above. We also indicated with full symbols the threshold velocity above which peripheral fragmentation (described in fig. 6) takes place: $\blacksquare$ $\ell = 3\,\mu$m ($h = 12$, 17, 26 μm); $\bullet$ $\ell = 4\,\mu$m ($h = 29$, 37, 43 μm).

than ℓ). Equating this pressure with the dynamic one yields: $\delta \sim \rho V^2 \ell^2/\gamma$. If δ becomes larger than h, the drop reaches the bottom surface, which is our criterion for impalement in the forest of pillars. Thus, for a given liquid and surface design, we get that pinning might occur if the velocity satisfies the inequality

$$V > V^* = (\gamma h/\rho \ell^2)^{1/2}. \tag{1}$$

Owing to the microscopic dimensions of the pillars, the critical velocity in eq. (1) may be quite large: for dimensions of typically 10 μm and for water, we find V^* of about 3 m/s, of the order of the terminal velocity of a millimetric raindrop. For larger microstructures, similar pinning transitions are observed, yet for much smaller impact velocities [12]. Hence, the reduction in size of the microtextures appears to be a condition for building robust water-repellent materials, that is, still efficient at large impact velocities.

Surprisingly, the scaling proposed in eq. (1) is found to describe the data even if the pillar height is larger than the inter-pillar distance. In the case of still larger values of the ratio h/ℓ, corresponding to dense forests of high pillars ($\ell = 2\,\mu$m, $h = 10\,\mu$m; $\ell = 3\,\mu$m, $h = 26\,\mu$m; $\ell = 4\,\mu$m, $h = 37\,\mu$m and 43 μm), we could not observe any pinning, whatever the impact velocity, demonstrating that it is possible to achieve a robust water repellency with such model super-hydrophobic solids. It would be interesting to see how our conclusions adapt to more complex designs (including natural ones), as very rough materials [1] or solids with a dual microstructure [13]: the determination of V^* provides a convenient and useful criterion for qualifying the water repellency of a super-hydrophobic substrate. It would also be worth quantifying what defines the size of the trapped region (as observed in fig. 3), as a function of impact velocity and of the nature of the design —an issue where numerical simulations might aid understanding [14]. The numerical coefficient deduced from the data (that is, about 0.05, significantly smaller than 1) also remains to be understood.

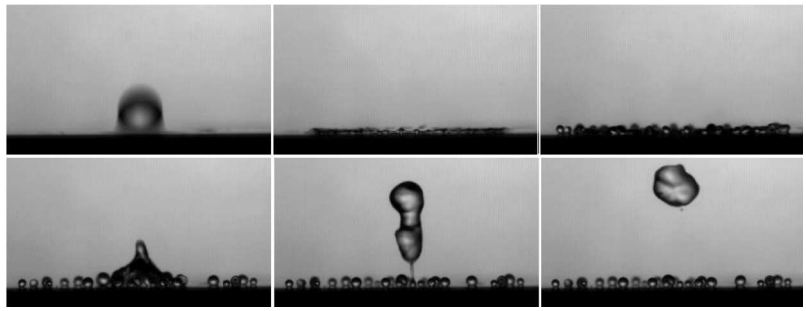

Fig. 6 – Side view of a millimetric water drop impacting a water-repellent surface ($h = 37\mu$m and $\ell = 3\,\mu$m) at a high speed ($V = 4.3$ m/s), just above the threshold of peripheral fragmentation: as the drop reaches its maximal extension, fingers appear and decay in droplets of about 200 μm of radius. This instability does not prevent the main drop (about 80% of the initial volume) from bouncing off. The ejected droplets remain at the top of the microstructures, evidencing a robust static water repellency. The times corresponding to the different snapshots are $t = 0$, 1, 3, 7, 15 and 23 ms.

The observation of bouncing drops at "high" impact velocities allowed us to notice an interesting fact. It is observed that the shock produces peripheral satellites, provided the impact velocity exceeds some threshold noted with full symbols in fig. 5 and independent of the texture characteristics. We displayed in fig. 6 a sequence of pictures showing this instability: the rim (visible in fig. 3) bounding the spreading liquid sheet destabilizes in droplets, which are left behind in the retraction stage. These droplets do not impale in the texture, owing to the characteristics of the pillars ($h = 37\,\mu$m and $\ell = 3\,\mu$m): strong water repellency also prevents small droplets from sinking, contrasting with what can be observed with shorter posts [5].

The threshold of satellite ejection is about 3.3 m/s for a water drop of radius $R = 1.1$ mm, corresponding to a Weber number $\rho V^2 R/\gamma$ of about 160. This value is much lower than that found on a hydrophobic flat solid, for which we observed a critical Weber number of about 700 for droplet ejection; on a flat hydrophilic solid, we could not observe any fragmentation of this kind (the Weber number being limited in our experiments to 1000). This emphasizes the role of the film of air, which is only present with super-hydrophobic solids: its presence minimizes the viscous dissipation in the spreading film, which remains fast as it extends; it thus thins considerably, allowing the formation and destabilization of a "free" rim at the border, as for a liquid sheet obtained by making a jet impact on a small solid target. This contrasts with "usual" solids, for which a strong viscous dissipation takes place close to the moving contact line (and it is all the stronger since the solid is hydrophilic), which slows down the drop, preventing this instability from taking place. The resulting satellites are found in fig. 6 to be quite monodisperse: we could naively think that their size scales as the thickness of the spread drop, but the mechanism for the drop size selection might be more complex, as shown on liquid sheets [15]. Since our system favors the emission of satellite droplets (which might be a practical issue in water repellency), we intend to use it for studying more carefully the poorly understood question of liquid fragmentation.

* * *

We thank D. Bartolo and S. Moulinet for many exchanges, C. Clanet, C. Gay, K. Okumura and D. Richard for discussions, and Essilor for financial support.

REFERENCES

[1] Onda T., Shibuichi S., Satoh N. and Tsujii K., *Langmuir*, **12** (1996) 2125.
[2] Bico J., Marzolin C. and Quéré D., *Europhys. Lett.*, **47** (1999) 220.
[3] Öner T. and Mccarthy T. J., *Langmuir*, **16** (2000) 7777.
[4] Yoshimitsu Z., Nakajima A., Watanabe T. and Hashimoto K., *Langmuir*, **18** (2002) 5818.
[5] Lafuma A. and Quéré D., *Nature Mater.*, **2** (2003) 457.
[6] He B., Patankar N. A. and Lee J., *Langmuir*, **19** (2003) 4999.
[7] Feng X., Feng L., Lin M., Zhai J., Jiang L. and Zhu D., *J. Am. Chem. Soc.*, **126** (2004) 62.
[8] Sun T., Wang G., Feng L., Liu B., Ma Y., Jiang L. and Zhu D., *Angew. Chem. Int. Ed.*, **43** (2004) 357.
[9] Krupenkin T. N., Taylor J. A., Schneider T. M. and Yang S., *Langmuir*, **20** (2004) 3824.
[10] Richard D. and Quéré D., *Europhys. Lett.*, **50** (2000) 769.
[11] Biance A. L. *et al.*, to be published in *J. Fluid Mech.* (2006).
[12] Bartolo D. *et al.*, *Europhys. Lett.*, **74** (2006) 299 (this issue).
[13] Shirtcliffe N. J., Mchale G., Newton M. I., Chabrol G. and Perry C. C., *Adv. Mater.*, **16** (2004) 1929.
[14] Moulinet S. *et al.*, to be published (2006).
[15] Clanet C. and Villermaux E., *J. Fluid Mech.*, **462** (2002) 307.